SANDIA REPORT

SAND2018-10380
Unlimited Release
Printed September, 2018

LDRD Project Number: 209699
LDRD Project Title: Feasibility of Single-sided 3D elemental imaging

Team Members: Melinda Sweany, Mark Gerling, Peter Marleau, and Mateusz Monterial (LLNL)

Prepared by
Sandia National Laboratories
Albuquerque, New Mexico 87185 and Livermore, California 94550

Sandia National Laboratories is a multimission laboratory managed and operated by National Technology and Engineering Solutions of Sandia, LLC., a wholly owned subsidiary of Honeywell International, Inc., for the U.S. Department of Energy?s National Nuclear Security Administration under contract DE-NA0003525.

Sandia National Laboratories

Issued by Sandia National Laboratories, operated for the United States Department of Energy by Sandia Corporation.

Available to DOE and DOE contractors from
U.S. Department of Energy
Office of Scientific and Technical Information
P.O. Box 62
Oak Ridge, TN 37831

Telephone: (865) 576-8401
Facsimile: (865) 576-5728
E-Mail: reports@adonis.osti.gov
Online ordering: http://www.osti.gov/bridge

Available to the public from
U.S. Department of Commerce
National Technical Information Service
5285 Port Royal Rd
Springfield, VA 22161

Telephone: (800) 553-6847
Facsimile: (703) 605-6900
E-Mail: orders@ntis.fedworld.gov
Online ordering: http://www.ntis.gov/help/ordermethods.asp?loc=7-4-0#online

SAND2018-10380
Unlimited Release
Printed September, 2018

LDRD Project Number: 209699
LDRD Project Title: Feasibility of Single-sided 3D elemental imaging

Melinda D. Sweany Mark D. Gerling Peter A. Marleau
Mateusz Monterial (LLNL)

Abstract

We present single-sided 3D image reconstruction and neutron spectrum of non-nuclear material interrogated with a deuterium-tritium neutron generator. The results presented here are a proof-of-principle of an existing technique previously used for nuclear material, applied to non-nuclear material. While we do see excess signatures over background, they do not have the expected form and are currently un-identified.

Acknowledgment

This work was funded under LDRD Project Number 209699 and Title “Feasibility of Single-sided 3D elemental imaging”. The team would like to thank fellow 08647 staff member Heather Seipel for going above and beyond in getting our laboratory up and running.

Contents

List of Figures

Chapter 1

Introduction

There are many techniques and deployed systems designed to reconstruct the elemental constituents of a sample. Certain applications have operational constraints that do not allow the container, often thick metal, to be physically opened, requiring a method which can interrogate the sample through the container. For applications such as this, the state-of-the art system currently used in the field is the Portable Isotopic Neutron Spectroscopy System (PINS) from INL [1].

The current PINS system implemented in the field uses a Californium-252 neutron source to interrogate a sample, and measures the gamma radiation resulting from neutron capture interactions (n,g) and inelastic (n,ng) interactions with a germanium detector; the result is a highly resolved gamma spectrum that is used to reconstruct the elemental constituents of a sample. This information is used to determine the type of chemical agent and any explosives present. There are, however, many useful interactions that do not have an appreciable neutron interaction probability at the energies emitted from a Californium-252 source. D-T PINS addresses this by interrogating with a deuterium-tritium (D-T) neutron generator, which isotropically emits mono-energetic 14.1 MeV neutrons, extending the elemental reconstruction capabilities by increasing the suite of available gamma lines. Because D-T generators emit isotropically, background interactions from the surrounding environment can reduce the accuracy of the reconstruction.

Correlated fast neutrons emitted from the sample in this interrogation scenario are currently un-utilized, but carry additional elemental information. The emitted neutron energy in an inelastic interaction is a function of the incident neutron energy (14.1 MeV), the emitted gamma energy, and the known Q-value of the interaction. Therefore, the neutron spectrum provides additional constraints on the elemental composition of the sample. The MINER system [2] is a 16 channel stilbene scintillator-based neutron spectrometer and imaging system, and has been deployed in several exercises for its radiological imaging and spectroscopic capability. Neutron spectra from several fission sources is shown in Figure 1.1. The system is at TLR6, and deployment considerations such as portability, power consumption, and ease-of-use were considered in its design. By combining gamma spectroscopy (with e.g. LaBr3 detectors) with neutron spectroscopy in the same system, the reconstruction accuracy is potentially improved with shorter acquisition times. Time correlated neutron and gamma spectroscopy could reduce accidental backgrounds.

In addition, imaging promises to offer advanced future capabilities that may allow for mul-

tiple munitions to be analyzed simultaneously. We have recently demonstrated a single-sided 3D imaging capability using correlated (n,g) emissions: using the measured time between correlated gamma-rays and neutrons, the distance to each inelastic interaction is estimated allowing for the reconstruction of the 3D distribution of each element present. Given our demonstrated imaging resolution of 4 cm, multiple munitions could be interrogated at the same time. Figure 1.2 demonstrates 3D imaging of two fission sources using the MINER system. In addition, because this imaging modality does not require access to both sides of a sample, munitions could be interrogated half-buried in the ground. Depending on the imaging resolution, this could enable elemental imaging within a munition, which would aid in characterization scenarios in which the integrity of the munition is damaged.

As a first step in demonstrating both the single-sided 3D imaging technique and the neutron spectrum reconstruction applied to non-nuclear material, we have performed a series of measurements using the MINER system on graphite samples, interrogated with a D-T neutron generator. The results as well as any additional detector characterization required for the measurements are presented below.

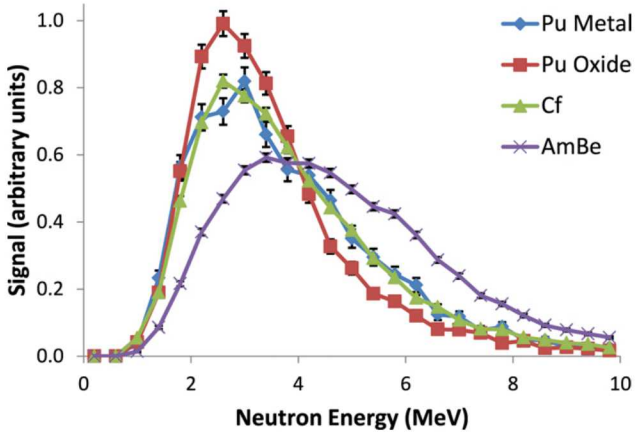

Figure 1.1: Area-normalized double-scatter spectra (not corrected for instrument response) for four neutron sources. The error bars represent one standard deviation statistical error, assuming a Poisson distribution in the number of events in each histogram bin. Taken from [2].

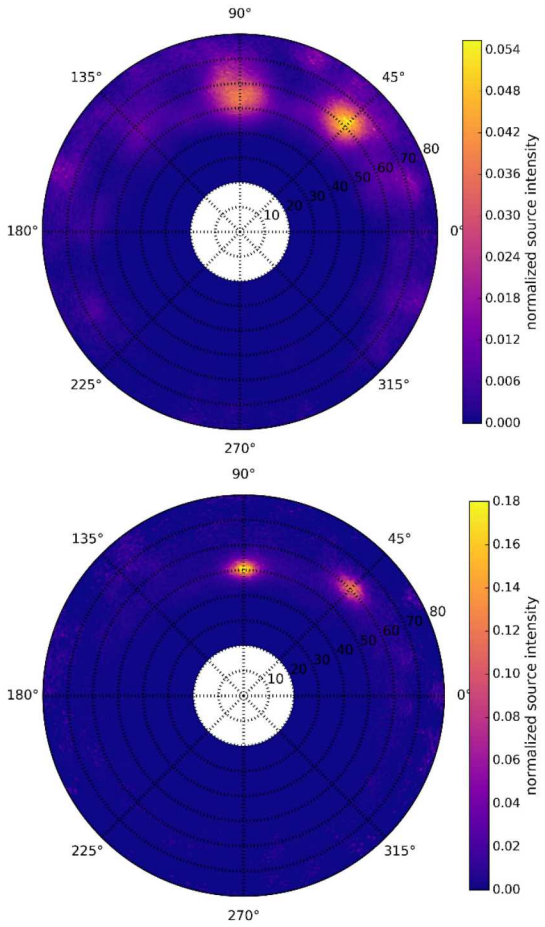

Figure 1.2: The polar projection (top-down view) of the image reconstruction for both an (top) experimental measurement and (bottom) simulation. Taken from [3].

Chapter 2

Detector Response and Calibrations

Although the MINER system has been well-characterized previously [2], there are some adjustments required on the data acquisition due to the higher energy depositions expected from D-T interrogations compared with fission energy neutrons. Specifically, the digitizers that acquire the data were currently using a 2 V scale for improved energy resolution. However, because D-T neutrons extend out to 14 MeV (compared with about 4 MeV for fission energy neutrons) some adjustments to both the PMT gain and the digitizer scale where necessary. Due to neutron quenching in the stilbene scintillator, 14 MeV neutrons are expected to deposit at most approximately 8 MeVee (MeV electron-equivalent). We calibrated the energy scale using the 4.4 MeV gamma line from an AmBe source, which is about half of the range to accommodate 8 MeVee. The gain on the individual PMT was adjusted so that the Compton edge from the 4.4 MeV gammas at 4.2 MeV occurs at approximately half of the full scale. Each tube is then calibrated further offline with an individual conversion factor that converts the output from the digitizers (ADC units) into energy units (keV). The calibrated energy spectrum from an AmBe source for all 16 cells is shown in Figure 2.1.

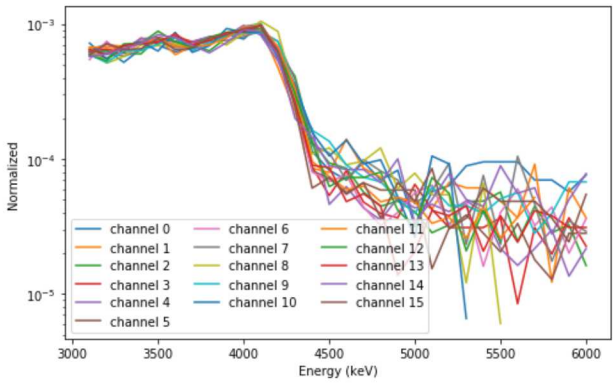

Figure 2.1: Calibrated energy spectrum of all 16 detector cells in MINER from AmBe gammas, showing the Compton edge of 4.4 MeV gammas at 4.2 MeV.

Once each channel is calibrated in energy, the pulse shape discrimination (PSD) must also be re-calibrated. Scintillation induced by gamma particles have a shorter decay time compared to scintillation induced by neutrons. In order to distinguish neutron and gamma depositions, we define a pulse shape parameter as the ratio of the pulse tail integral to the total pulse integral:

$$\text{psd} = \frac{\sum_{s=c}^{s=d} |A_s|}{\sum_{s=b}^{s=d} |A_s|}, \tag{2.1}$$

where A_s is the amplitude at sample s. The tail window is defined as $c \leq s \leq d$, and the total window is defined as $b \leq s \leq d$. The data acquisition system acquires gated data in which these windows were chosen to optimize PSD for fission energy neutrons. Due to the high data rate resulting from the D-T tube, we chose to continue to acquire gated data, rather than full waveforms. This may result in non-optimal PSD at higher energies, however there is still a strong ability to distinguish between neutron and gamma interactions. The (PSD) parameter as a function of deposited energy is shown in Figure 2.2, with the gamma population centered at approximately 1.1 on the y-axis, and the neutron population above. In order to determine the energy-dependent bounds of each population, we fit the projection of the PSD parameter in several energy slices to a double-gaussian distribution, and define a Bayesian probability based on the gaussian response:

$$\hat{P}_n(E) = \frac{\mathcal{L}_n(E)}{\mathcal{L}_n(E) + \mathcal{L}_\gamma(E_p) + \mathcal{L}_O}, \tag{2.2}$$

where the likelihoods are defined by the gaussian response at a particular energy. Because our calibration source is the same as our experimental data with minor changes in the scattering environment, the amplitude of the gaussian response is included to normalize the probability densities for the proper neutron to gamma ratio. Finally, an additional constant $\mathcal{L}_O$ is included for depositions that do not match either neutron or gamma characteristics. The resulting upper and lower bounds for neutron and gamma populations are shown as red dots in Figure 2.2.

As a check, we acquired data with no radiological sources present. The PSD vs. energy distributions which exceed the probability cut of gamma and neutron depositions are shown in Figure 2.3. For a background run, we expect few if any neutron depositions, and gamma depositions should be dominated by 1.4 MeV gammas from Potassium-40 and 2.6 MeV gammas from Thalium-208. The Compton edges at 1.2 MeV and 2.3 MeV, respectively, are visible in the energy projection of the gamma population.

Finally, the timing offsets between digitizer channels are calibrated using coincidences of gamma interactions between detector cells. Several calibrated timing offsets between cells, $t_a - t_b$, where a and b are individual cell numbers, are shown in Figure 2.4.

With the energy, pulse-shape discrimination, and timing response characterized, the system is fully calibrated and prepared to perform imaging and neutron spectroscopy measurements. The one exception to this is the exact form of neutron energy quenching for the stilbene. This response is taken from the literature, which has some disagreement. For these results, we have taken the curve from Kuchnir from Figure 2.5.

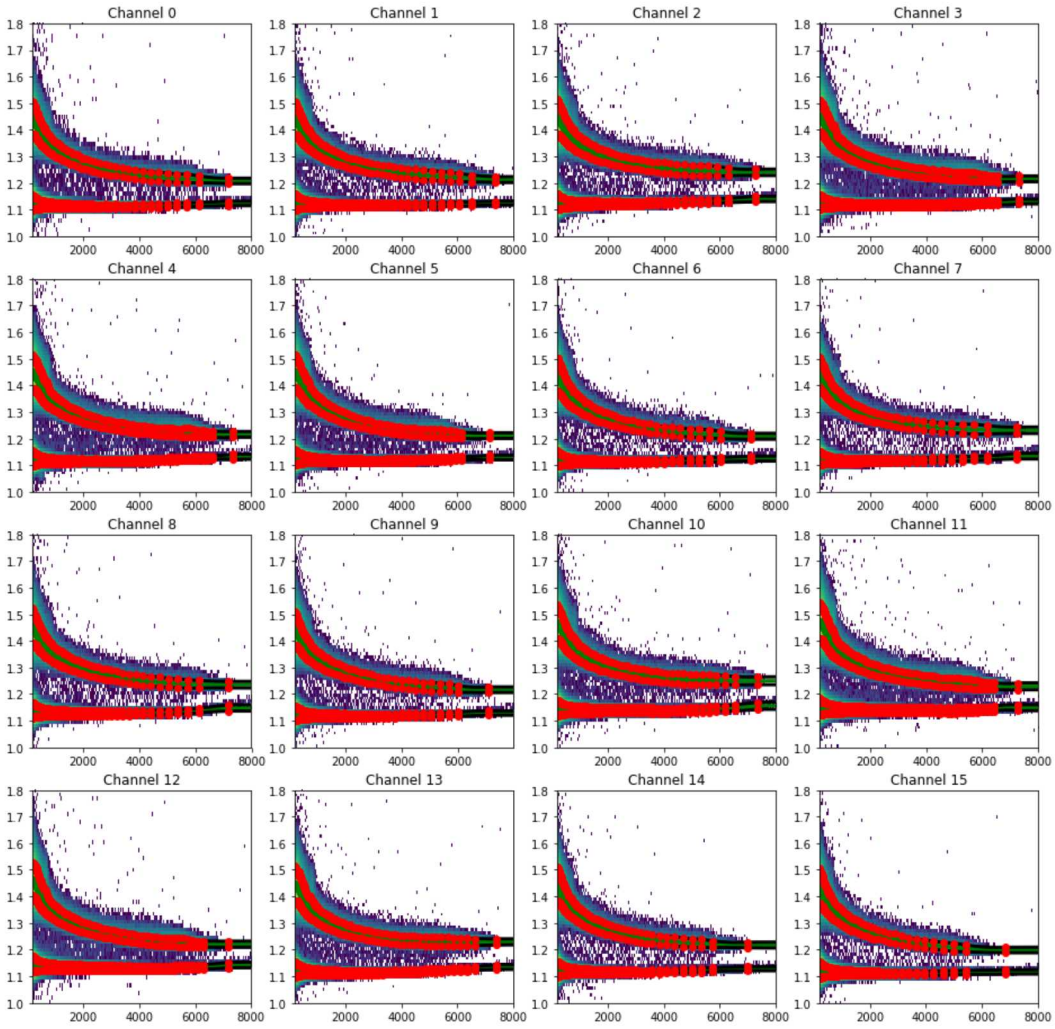

Figure 2.2: The pulse-shape discrimination calibration for all cells in MINER. The red dots indicate the upper and lower bounds of the neutron and gamma populations.

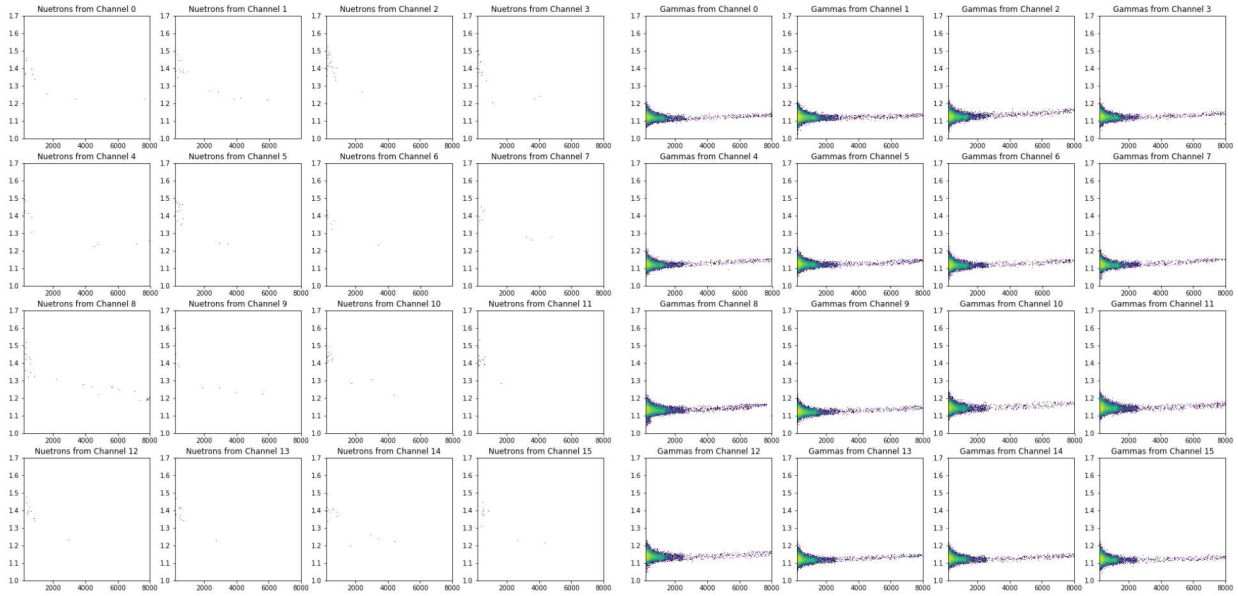

(a) (b)

Figure 2.3: The PSD as a function of energy for (a) neutrons and (b) gammas for a background acquisition. As expected for backgrounds, there are few if any neutron depositions, and the Compton edges from Potassium-40 (1.2 MeV) and Thalium-208 (2.3 MeV) are visible in the gamma population.

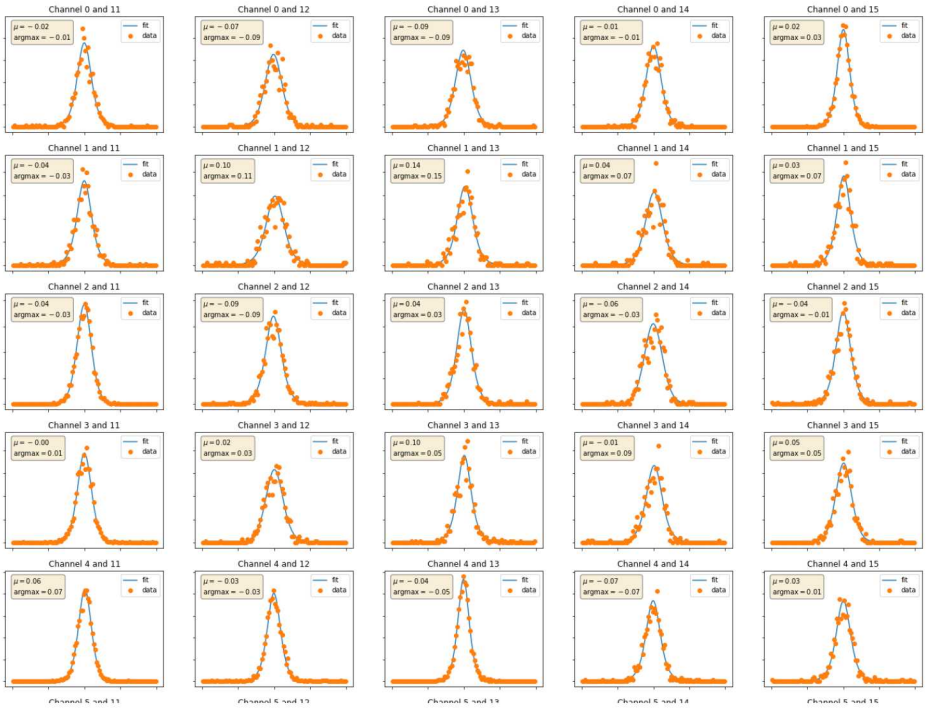

Figure 2.4: Example timing distributions for correlated gamma depositions between several channel pairs.

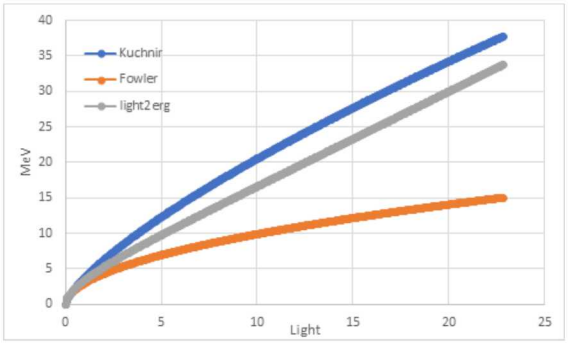

Figure 2.5: The neutron energy deposition vs. light output (in MeVee) for stilbene from various sources in the literature. The results presented here use the curve from Kuchnir.

Chapter 3

Imaging and Neutron Spectrum Results

The kinetic reconstruction of the neutron emissions, which with adequate statistics provides both a 2D map of the neutron emissions and their incoming energy spectrum, requires two neutron-proton elastic scatters: the neutron direction before the first scatter lies on a cone defined by the angle θ:

$$\cos(\theta) = \sqrt{\frac{E_{n'}}{E_n}}, \tag{3.1}$$

where E_n is the in-coming neutron energy and $E_{n'}$ is the neutron's energy after the first interaction. $E_{n'}$ is determined by the neutron time-of-flight ($t_{n-n'}$) and distance ($d_{n-n'}$) between the first and second neutron interaction:

$$E_{n'} = \frac{1}{2} m_n \left(\frac{d_{n-n'}}{t_{n-n'}} \right)^2. \tag{3.2}$$

Finally, the in-coming neutron interaction is determined by the energy deposited in the first interaction, E_p, measured by the light emitted in the first scintillation pulse, and $E_{n'}$:

$$E_n = E_{n'} + E_p. \tag{3.3}$$

Imaging in 3D is achieved by utilizing the measured time-of-flight difference ($t_{\gamma-n}$) between a gamma ray and the first neutron interaction, providing a relative distance between the simultaneously emitted gamma and neutron [3]:

$$\begin{aligned} R_n = (c^2 - v_n^2)^{-1} \Bigg[& c^2 t_{\gamma-n} v_n - d_{\gamma-n} v_n^2 \mu \\ & + \sqrt{v_n^2 \left(c^2 (t_{\gamma-n}^2 v_n^2 - 2 d_{\gamma-n} v_n \mu t_{\gamma-n} + d_{\gamma-n}^2) + v_n^2 d_{\gamma-n}^2 (\mu^2 - 1) \right)} \Bigg], \end{aligned} \tag{3.4}$$

where

$$\mu = \frac{\overrightarrow{n\gamma}}{d_{\gamma-n}} \cdot \hat{R}_n(\phi). \tag{3.5}$$

is the cosine of the angle between the surface of the cone of possible source locations and the vector $\overrightarrow{n\gamma}$ defined by the neutron and gamma interaction locations. The analysis therefore requires a triple coincidence between one gamma and two neutron interactions, in contrast to the double neutron coincidence required for 2D imaging.

In order to evaluate both the neutron TOF spectrum and 3D imaging of carbon, we acquired three separate data runs with MINER and a D-T neutron generator. In both cases, the D-T generator is 132 cm away from the center of the MINER instrument, and is at approximately 5 degrees in the MINER reference frame. The first data run was acquired with no carbon sample present, in order to obtain a background measurement which will allow us to evaluate the spectral response of room return and obtain an image of possible carbon background sources in the room. To reduce these effects as much as possible, the D-T tube was placed 94 cm off the ground, and the area was cleared of high mass objects that were not necessary for the measurement. In order to reduce accidental neutron gamma coincidences, a stack of lead bricks were placed between the D-T tube's target and the photodetectors inside MINER, so that approximately 3 inches of lead shielding is between MINER and the target. A large foam block was also in place for a graphite sample to stand on in a later run. In this configuration, 8 hours of data were obtained.

Next, three cylindrical bottles of graphite, each 7.62 cm in diameter and 12.7 inches tall and a combined 510 grams, were placed at 22 degrees in the MINER reference frame, 109 cm away from the center of MINER. Figure 3.1a shows the experimental setup with the graphite sitting next to the stack of lead (green blocks). Another 8 hours of data were obtained in this configuration. Finally, the three graphite bottles were placed on the foam block at -80 degrees and 69 cm away. We obtained 8 hours of data in this configuration. Figure 3.1b shows the experimental setup for this configuration, with the graphite sitting on top of the foam block.

Figure 3.2 shows both the raw and background subtracted incoming neutron spectrum from the two graphite runs and the background run. The background subtracted graphite spectra show an excess of events above 14 MeV, which could suggest some instability in the output of the neutron generator, but could also result from low angle scattering off of adjacent material. D-T tube instability should result in an energy independent offset, however if the output for the graphite run was lower, it could create negative bins in the background subtracted spectrum. We do not expect neutron energies above 14 MeV, so it is likely that the energy quenching formula is inaccurate. The dataset with the graphite placed closest to MINER has an additional population below 4 MeV: this is possibly the inelastic neutron interactions off of carbon. It may also be due to an increase in room return background, or neutrons scattering from the floor and other room objects, in the case that the output from the DT tube is not stable: these should again cause an energy-independent offset. Figure 3.3 shows the outgoing neutron energy resulting from carbon interactions and depositing energy in a 3 inch detector cell. In our experimental setup. A comparison

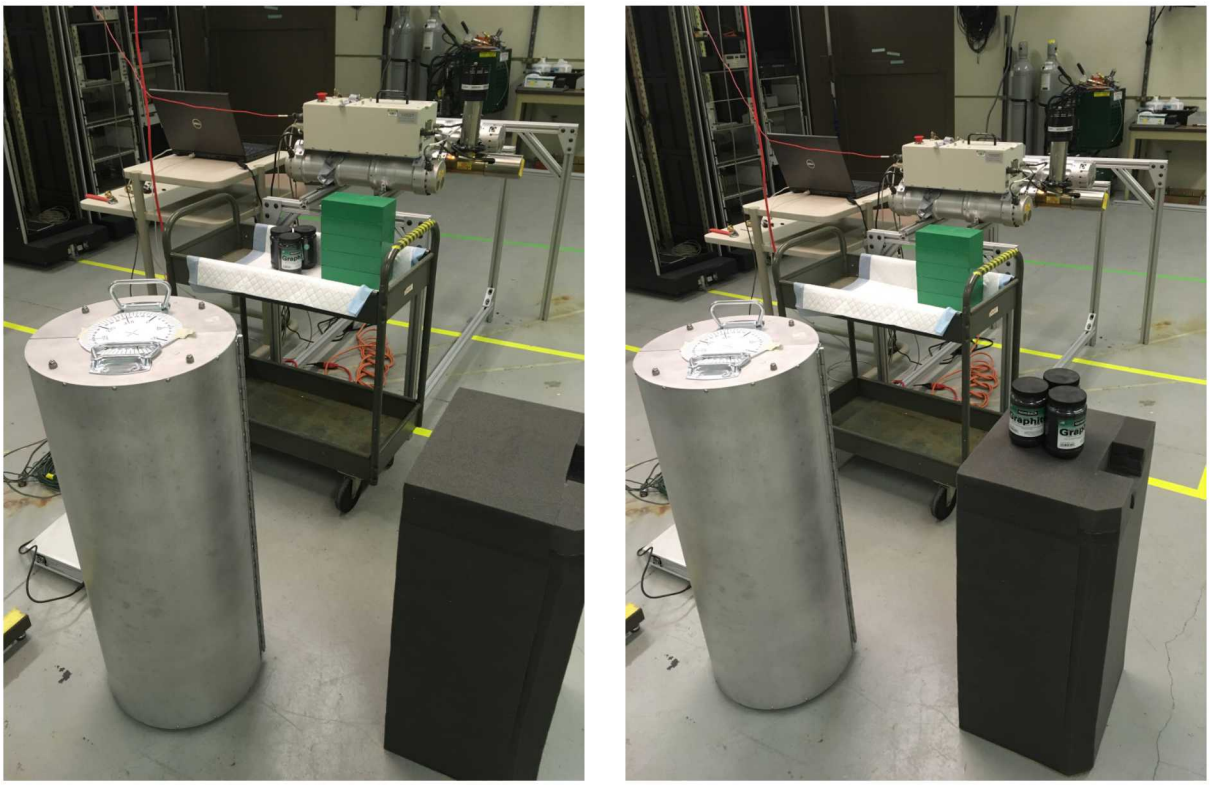

(a) (b)

Figure 3.1: (a) Graphite measurement configuration 1: the graphite is at 22 degrees in the MINER reference frame, and the D-T tube is at 8 degrees. The graphite is ∼112 cm away from the center of the MINER instrument, and the D-T tube is 132 cm away. (b) Graphite measurement configuration 2: the graphite is at -80 degrees in relation to the MINER reference frame, and the D-T tube is at 8 degrees. The graphite is ∼68.5 cm away from the center of the MINER instrument, and the D-T tube is 132 cm away.

of Figures 3.2 and 3.3 suggests that we may be seeing inelastic neutron interactions off of carbon, in addition to elastic scattering, however this is not strong evidence of our expected signal.

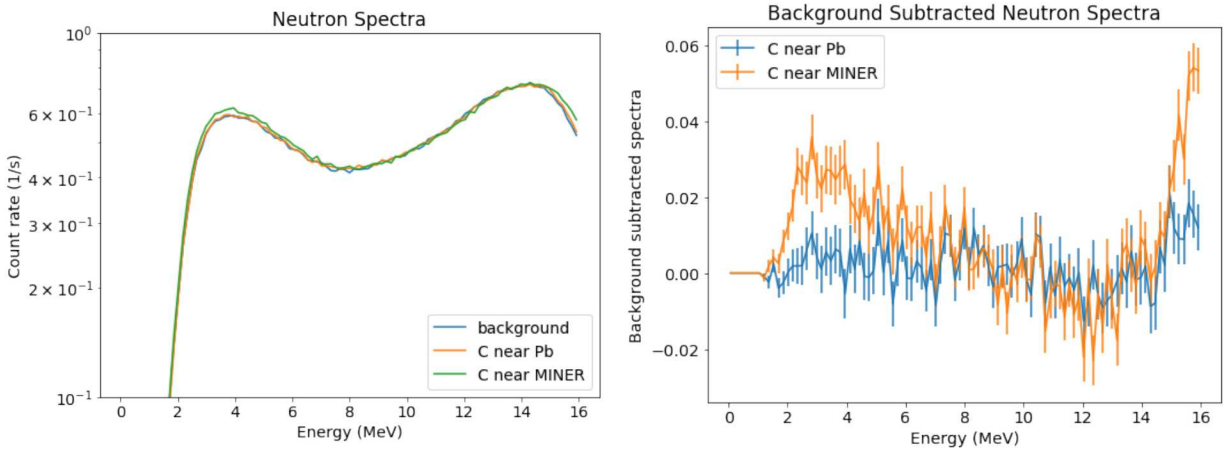

(a) (b)

Figure 3.2: The neutron incoming spectrum for (a) all three datasets and (b) the graphite datasets with the background run subtracted.

The 2D reconstructed images for all three datasets are shown in Figure 3.4. Neither result shows a strong signal apart from the 14 MeV neutron emission from the DT tube. The background subtracted images in Figure 3.5 also do not show a strong source for either graphite run. Finally, the 3D images (Figure 3.6) and the neutron spectrum for triple coincidences (Figure 3.7) show a slight excess for the run with the graphite near MINER. It is interesting to note the comparison between the neutron spectrum correlated with gammas (Figure 3.7) and not correlated with gammas (Figure 3.2): imposing the gamma correlation eliminated the high-energy contribution, presumably from elastic neutron scatters, which is expected since these events do not produce a correlated gamma.

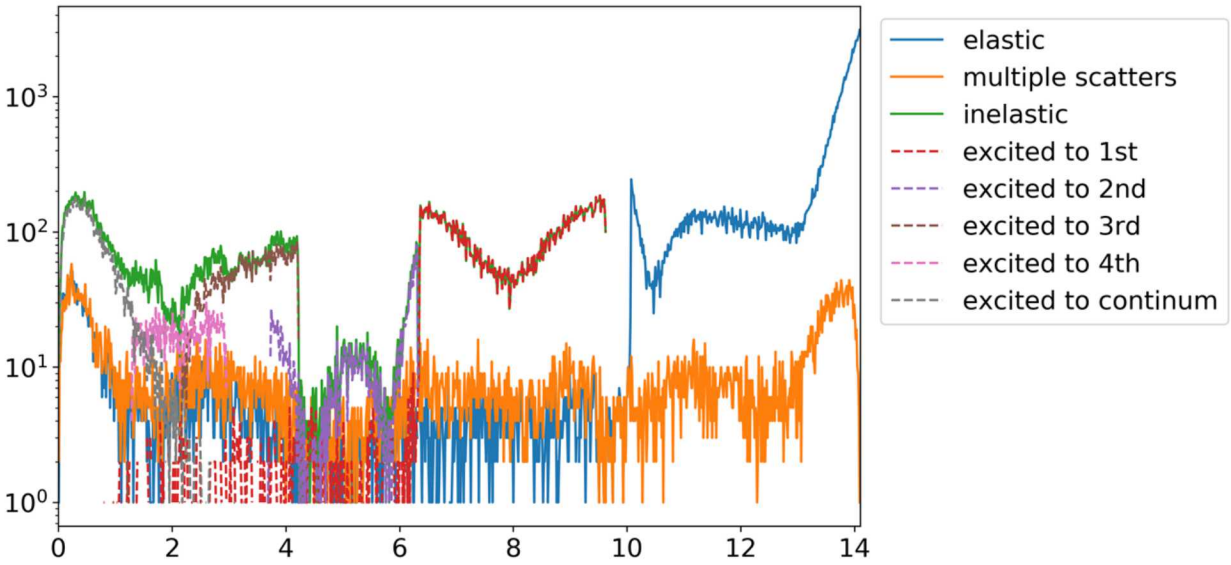

Figure 3.3: The simulated neutron spectrum from 14 MeV neutrons scattering off of a carbon target and depositing energy in a 3 inch detector cell 50 cm away.

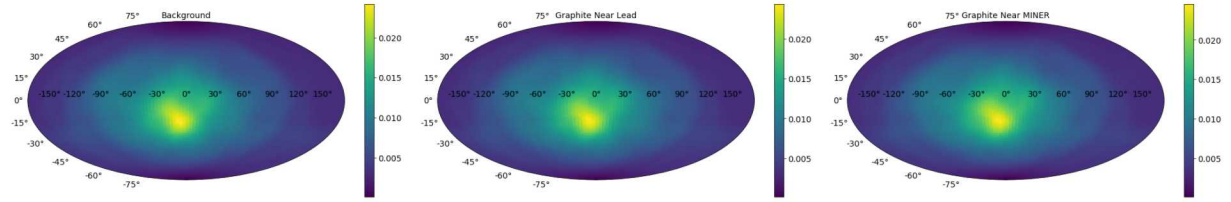

(a) (b) (c)

Figure 3.4: The 2D image reconstruction for (a) background (b) the graphite far from MINER and (c) the graphite near MINER.

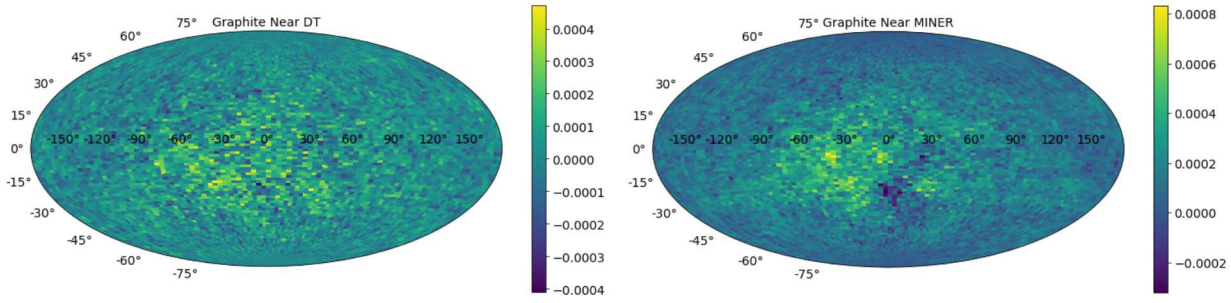

(a) (b)

Figure 3.5: The 2D, background subtracted images for (a) the graphite far from MINER and (c) the graphite near MINER. The images are projected at a distance of 112 cm, and no difference was observed for other projection distances.

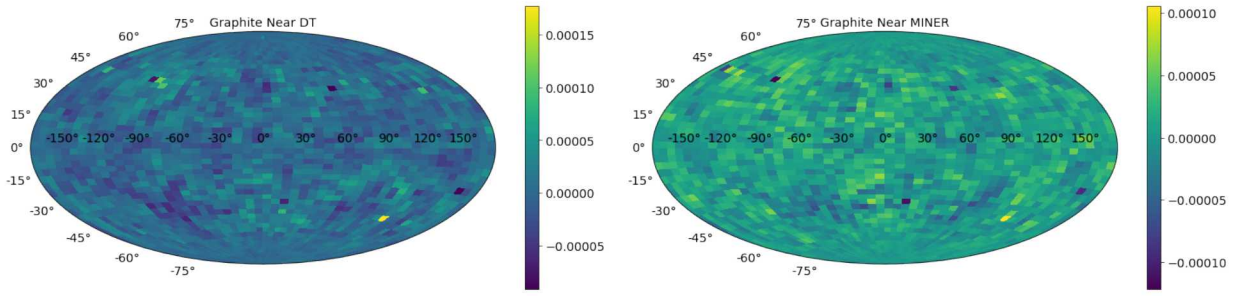

(a) (b)

Figure 3.6: The 3D projected images (background subtracted) for (a) the graphite far from MINER and (b) the graphite near MINER.

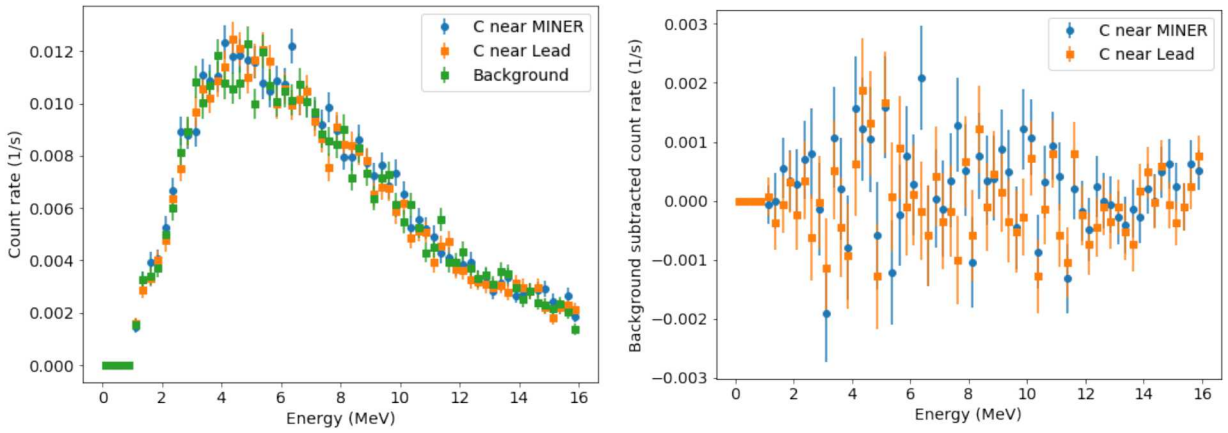

(a) (b)

Figure 3.7: The neutron spectrum from triple coincidences (gamma, neutron, neutron) (a) raw and (b) background subtracted.

Chapter 4

Discussion and Conclusion

In an effort to extend our recently demonstrated single-sided imaging technique to non-radiological material, and also to measure the neutron spectral response from inelastic neutron interaction, we deployed a neutron imaging system to measure neutron interactions from a carbon source interrogated with a D-T neutron source. While we do observe some excesses over background, and these could plausibly be from inelastic scattering, there is no obvious signal that matches our expectations. It may be that we are dominated by multiple carbon scatters within the sample, in which case a smaller sample may produce more clear results (see Figure 3.3). The data may suffer from two effects that are masking the signal. First, the neutron energy quenching formula may be incorrect, causing the neutron energy spectrum to be distorted. In this instance, we would see excesses over background, but the features will be at the incorrect energies. The second more likely problem is that our signal is overwhelmed by the room return background.

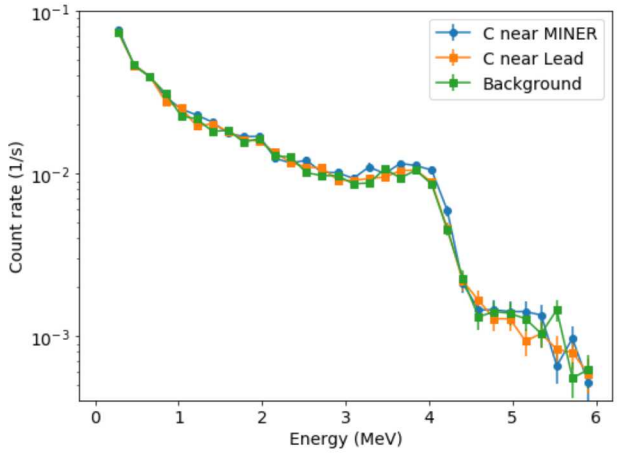

Figure 4.1: The gamma spectrum for events with a gamma/neutron/neutron coincidence. All datasets clearly show a Compton edge from 4.4 MeV gammas, expected from inelastic scatter off of carbon.

Another irreducible background in these measurements is the detector itself, which is composed of organic scintillator containing large amounts of carbon. Figure 4.1 shows the gamma spectrum from events that are triple coincidences (gamma-neutron-neutron), and clearly shows a Compton edge in all datasets at 4.2 MeV, expected from the 4.4 MeV

gamma resulting from neutron inelastic scattering off of carbon. Because this is so strong in all runs including the background, we suspect these are due to interactions in the detector medium. While this won't show up in a background subtracted spectrum, it may be masking the smaller signal from our graphite sample. An API would greatly reduce this effect as well.

If this is the case, repeating the experiment with an associated particle imaging capable D-T neutron generator (API D-T) would greatly improve our ability to eliminate neutron emissions from the tube that do not intersect the vicinity of our intended target. This is a greater effort that is not within the scope of this existing project, and would require a time correlated signal from the API to the MINER data acquisition system.

References

[1] E.H. Seabury and A.J. Caffrey "Explosives Detection and Identification by PGNAA" *INL/EXT-06-01210* (2006)

[2] J.E.M. Goldsmith, M.D. Gerling and J. S. Brennan *Review of Scientific Instruments* **87** (2016) 083307

[3] M. Monterial and S.A Pozzi "Single-View 3-D Reconstruction of Correlated Gamma-Neutron Sources" *IEEE Transactions on Nuclear Science* **64** (2017) 1840-1845

DISTRIBUTION:

1	MS 0899	Technical Library, 8944 (electronic copy)
1	MS 0359	D. Chavez, LDRD Office, 1911

Sandia National Laboratories